Maderas-Cienc Tecnol 26(2024):12, 1-30
Ahead of Print: Accepted Authors Version

DOI:10.4067/S0718-221X2024005XXXXXX

ASSESSMENT OF CELLULOSE NANOFIBERS FROM BOLAINA BLANCA WOOD OBTAINED AT THREE SHAFT HEIGHTS

Sergio Andre Arango-Perez[1*] https://orcid.org/0000-0001-8837-7301

Héctor Enrique Gonzales-Mora[1] https://orcid.org/0000-0002-8455-3432

Silvia Patricia Ponce-Alvarez[2] https://orcid.org/0000-0003-1583-7113

Abel Aurelio Gutarra-Espinoza[2] https://orcid.org/0000-0002-4955-419X

Aldo Joao Cárdenas-Oscanoa[1*] https://orcid.org/0000-0003-3093-8414

[1]Universidad Nacional Agraria La Molina, Facultad de Ciencias Forestales, Departamento de Industrias Forestales, Laboratorio de Productos Forestales de Transformación Química, Lima, Perú.
[2]Universidad de Lima, Grupo de Nanomateriales Aplicados, Lima, Perú.

***Corresponding author:** sarango@lamolina.edu.pe
Received: October 08, 2022
Accepted: September 27, 2023
Posted online: September 28, 2023

ABSTRACT

This study evaluated cellulose nanofibers from bolaina blanca wood (*Guazuma crinita*) obtained at different heights of the longitudinal axis of the shaft of trees from a three-and-a-half-year-old plantation. The wood was subjected to pulping, bleaching and subsequent mechanical milling using a Changsha Samy XYQM-2L planetary ball mill to obtain cellulose nanofibers. The product was characterised using analytical techniques: scanning electron microscopy, X-ray diffraction, thermogravimetric analysis, Fourier transform infrared spectroscopy, ultraviolet–visible spectroscopy. Additionally, the degree of polymerisation was determined. The effect of longitudinal position on cellulose nanofibers characteristics was evaluated by comparing means using ANOVA and Kruskal–Wallis statistical tests. The yield of cellulose nanofibers production from the high, middle and basal sections was 32,1 %, 33,6 % and 31 %, respectively. The obtained cellulose nanofibers exhibited a significantly larger diameter for the high zone (84 nm) compared with the middle (75 nm) and basal (69 nm) zones; the length remained above the micrometre range. With respect to degree of polymerisation, a decrease was evidenced with respect to the increase in shaft height; the basal zone exhibited a degree of polymerisation of 300, a significantly higher value than the middle and high zones, which exhibited degree of polymerisation of 249 and 211, respectively. The product showed typical cellulose type I polymorphism and crystallinity indexes of 76 %, 93 % and 96 % for the high, middle and basal sections, respectively. Regarding the thermostability of cellulose nanofibers, the maximum degradation rate of cellulose nanofibers occurred between 335 °C and 341 °C, with cellulose nanofibers from the basal area being the most stable. The adsorption of the methylene blue dye on cellulose nanofibers was evaluated; an efficiency > 60 % was found.

Keywords: Bolaina blanca, cellulose nanofibers, polimerization degree, *Guazuma crinita*, pulp treatment.

INTRODUCTION

Cellulose is the most abundant renewable polymer on the planet, with an annual biosynthesisation estimated at > 1011 tonnes (Habibi 2014). Owing to its natural origin and widespread availability, cellulose is used in fibre form or derived form for creating a wide range of materials and products, such as paper, composite boards, cosmetics, and food additives.

Cellulose fibre is represented at different levels. From a biological viewpoint, cellulose chains are formed by β-D-glucose units. The second level or macromolecular level comprises the union of these linear cellulose chains with each other forming the elementary fibrils or microfibrils, also known, from a technical-technological point of view, as nanocellulose. The extraction of these nanoconstituents is possible using mechanical and chemical methods or using a combination of these methods (Borjesson and Westman 2015, Kargarzadeh *et al.* 2017, Siddiqui *et al.* 2011, Yildirim and Shaler 2017).

Nanocellulose (NC) has become extremely popular in different industries not only for being a biodegradable material with high availability but also for possessing interesting properties, such as high mechanical strength and low density, dielectric properties, possibility of chemical modification, dimensional stability and thermal stability (Herrera 2018, Ozen *et al.* 2021, Tarres 2017). Due to these benefits, nanocellulose is a basic material used in different industries such as: Construction/polymers, Paper industry, Cosmetics, Biomedicine and Food industry (Herrera 2018, Lee *et al.* 2012, Tarres 2017).

However, there is still insufficient knowledge concerning the potential influence of raw material sources on the final characteristics of NC. Wood is one of the main sources currently used for NC production owing to its lignocellulose composition and high availability. The most commonly used forest species are Eucalyptus and Pine, but there

68 are also other alternatives such as tropical species that have adapted to a fast-growing
69 plantation system, which is ideal for the continuous production of NC.

70 In this context, assessing other non-conventional potential forest sources for the creation
71 of NC is an interesting research topic, while also posing the question of how the different
72 heights of the longitudinal axis of the shaft influence the characteristics of NC.

73 Among the species used for plantation purposes, bolaina blanca (*Guazuma crinita*) stands
74 out (Miguel *et al.* 2019, Rodríguez *et al.* 2015). This forest species is widely cultivated
75 in the country owing to its advantage of being a fast-growing species harvestable at an
76 early age as well as the large demand for its wood for construction, furniture and
77 mouldings (Revilla 2015).

78 Considering the production potential of bolaina blanca wood as a premise, promoting its
79 use for the creation of products other than timber is necessary. All this to create products
80 with added value in a world market that indicates a trend in biodegradable products to
81 reduce global pollution, besides reusing or disposing waste in other ways owing to its
82 organic origin (Trache *et al.* 2020).

83 ## MATERIALS AND METHODS

84 ### Collection and preparation of raw material

85 The material was extracted from three randomly selected trees with no signs of disease
86 from a three-and-a-half-year-old plantation located in the province of Padre Abad,
87 Department of Ucayali, Peru. A total of 58 kg of debarked bolaina blanca wood (*Guazuma*
88 *crinita* Mart.) corresponding to logs from the basal, middle and high zones was collected.
89 Heights were assigned based on the division of the commercial length of the shaft of the
90 tree.

Wood samples were subjected to natural drying up to a humidity of 20 %. The material was chipped to obtain chips with 15 mm length and 5 mm width. A total of 7 kg of wood extracted from the most central part of each of the basal, middle and high sections was used.

Chemical characterisation of bolaina blanca wood

The wood was sawed according to the origin of the longitudinal section to obtain sawdust, which was sieved and prepared for chemical characterisation tests. The content of the extractives was determined according to the TAPPI T 204 cm-97 standard (Tappi 2007), using 96 % ethyl alcohol for extraction. The holocellulose and cellulose contents were obtained using the Jayme–Wise and Kurnchner-and-Hoffer methods, respectively. Hemicellulose content was found by subtracting holocellulose and cellulose contents.

Lignin content was determined using the Klason method according to the TAPPI T 222 om-98 standard (Tappi 1998). Moreover, the TAPPI T 211 om-93 standard was used for ash (Tappi 1993).

Obtaining and bleaching cellulosic pulp

The cellulosic pulp was obtained via alkaline digestion. This process was performed in triplicate for each section of interest, using a total of 5,4 kg of dry wood mass.

A total of 600 g of dry mass of wood chips for each section of study were moistened via immersion for 24 hours at room temperature, prior to the cooking process. Cooking was conducted using 18 % NaOH and 0,1 % anthraquinone (percentages corresponding to the dry mass of wood), a liquor/wood weight ratio of 4:1 and an H-factor of 1200. The pulping was conducted in a 15 L rotary digester at a defined pressure from 6 kg/cm^2 to 10 kg/cm^2 and a maximum temperature of 180 °C for 3 hours. The chemical pulping yield was determined after washing the pulp.

The bleaching process was conducted on approximately 2,4 kg total dry mass of cellulosic pulp obtained previously.

The pulps were bleached in polyethylene bags placed in a water bath and underwent a sequence of four bleaching stages. Table 1 shows the parameters used during the bleaching stages.

Table 1: Bleaching sequence.

SEQUENCE / REAGENT	**D** (ClO_2)	**E** (NaOH)	**H** (NaClO)	**P** (H_2O_2)
No. of repetitions	2	1	1	1
Bleach distribution (%)	6	5	20	2
Temperature (°C)	70	70	45	70
Time (minutes)	60	120	150	90
Consistency (C%)	8	8	8	10
pH	< 4	> 11	9 – 11	10 – 11

Note: Bleach distribution corresponds to percentage of the dry mass of the pulp. At the end of each sequence, the pulp was washed with deionised water to neutralise the reagents used. Approximately 32 L of deionised water was used.

The amount of residual lignin in the pulps obtained before and after bleaching was evaluated using the micro-Kappa index according to the TAPPI T 236cm-85 standard (Tappi 1993b).

Measurement of anatomical elements of interest in fibres of *Guazuma crinita*

The anatomical characterisation of bolaina blanca fibres was performed from the cellulosic pulp. The length, width and wall thickness of 30 fibrous bundles were evaluated. This evaluation was performed according to the standard procedures for wood anatomy studies (IBAMA 1991) using a LEICA DM500 microscope at 4X, 10X and 40X magnifications.

Obtaining and lyophilising cellulose nanofibers (CNF)

CNF was obtained from the bleached pulp exposed to a 1 % consistency in water, via mechanical defibrillation using a Changsha Samy planetary ball mill model XYQM-2L,

grinding speed of 300 revolutions per minute (rpm), total time of 3 hours and centripetal force of approximately 360 N.

After grinding, the obtained CNF was subjected to freeze-drying for yield calculation and characterisation. It started with the conditioning of the material using a freezing bath at − 40 °C (230-V FRYKA cooling bath model KB 18-40). Freeze-drying was conducted at a reduced absolute pressure (3 Pa) for 20 hours in a Christ Alpha 1-2 LDplus 230-V freeze-dryer.

Characterisation of CNF

Determination of degree of polymerisation (DP) of CNF

DP was determined using a capillary viscometer (Ubbelhode) to calculate the intrinsic viscosity (ŋ) according to TAPPI T 230 om-08 (Tappi 2008).

Scanning electron microscopy

The morphological analysis of CNF was performed via scanning electron microscopy (SEM) using ZEISS EVO MA10 equipment. The samples were dried at 50 °C for 24 hours to determine the diameter of the fibres through the obtained images.

Fourier transform infrared spectroscopy

A Bruker Alpha II Fourier transform infrared spectrometer (FTIR) was used to analyse the molecular vibrations of the freeze-dried CNF samples for each longitudinal section of the tree.

The attenuated total reflection method was conducted with successive scans at a resolution of 4 cm^{-1} and wavelengths in the 400 cm^{-1} – 4000 cm^{-1} range. Data were processed using FTIR software.

X-ray diffraction

A Bruker D8 ADVANCE X-ray diffractometer was used. X-rays with a wavelength of 1,5406 Å were incident on the freeze-dried CNF, for each longitudinal section of the tree. In the analysis parameters, the Bragg angle was swept in the range $6^o \leq 2\theta \leq 90^o$ with an interval of 0,01º.

The percentage crystallinity was calculated using equation 1 according to Segal's method (Segal *et al.* 1959):

$$IC = \left(1 - \frac{I18}{I\ 22{,}6}\right).100 \quad (1)$$

where *IC* is the crystallinity index*; I*18 and *I*22,6 are intensities corresponding to the diffraction angles 2θ = 18° and 2θ = 22,6°, which in turn correspond to the reflection planes (110) and (200), respectively.

Moreover, the average size of the cellulose crystals was determined using the Scherrer equation (equation 2), calculated for the intensity corresponding to the crystallographic plane (200) (2 θ = 22,6°).

$$D = \frac{0{,}94\ \lambda}{b cos\theta'} \quad (2)$$

where 0,94 is the value of *Scherrer's* constant corresponding to the symmetry and shape of cellulose crystals, λ is the wavelength of the X-rays with a value of 1,5406 Å and *b* is the half-peak width (in radians).

Thermogravimetric analysis

Thermogravimetric analysis was performed individually for CNF from high and basal section using the TGA 70-LECO equipment according to ASTM D7582 (2015). Freeze-dried CNF samples weighing 1 g were placed in aluminium crucibles and subjected to analysis in the 25 °C – 900 °C range at a heating rate of 10 °C·min^{-1}.

Ultraviolet–visible (UV–Vis) spectroscopy

Measurements were performed using a Perkin Elmer Lambda 21 UV–Vis spectrophotometer to determine the adsorption capacity of lyophilised CNF for methylene blue dye. CNF was analysed at two concentrations of methylene blue, 10 ppm and 20 ppm. Methylene blue was used as a control dye because it is water soluble and easy to detect in spectrophotometric equipment (Lermen *et al.* 2021).

In each case, a 15-mL sample of the solution was collected and placed in a tube of the same volume in duplicate. The sample was then centrifuged for 30 min at 5000 revolutions per minute (rpm) to sediment CNF particles. The liquid fraction, without the sediment, was read using the spectrophotometer; moreover, blank readings were recorded.

Experimental design

The data analysis was conducted using the longitudinal height of the trunk as the only variable, exposed at three levels: basal, middle and high sections. Eventually, the mean values were compared.

The results were evaluated using analysis of variance and the Kruskal–Wallis test and, in case of significance, the Tukey and Mann–Whitney tests were performed at a confidence level of 95 %.

RESULTS AND DISCUSSION

Chemical characterisation of bolaina blanca wood

The results obtained showed no significance for macromolecular components such as cellulose, hemicellulose and lignin as well as for low molecular weight components such as extractives, ash and silica, along the longitudinal axis of the trunk for three-and-a-half-year-old bolaina blanca trees (Table 2). This indicates that the zone of the tree did not influence the contents of the chemical components of the extracted samples. The reported

values agree with those reported by Córdova *et al.* (2020) for similar species and age, and Cipra Rodriguez *et al.* (2022) for same wood from 5 to 8 years.

Table 2: Chemical composition (%) of sections of bolaina blanca wood.

Component (%)	High	Middle	Basal	Statistical test
Cellulose	53,30 (0,72)	52,67 (0,92)	52,54 (0,72)	ANOVA (n.s.)
Hemicellulose	24,18 (3,87)	23,76 (3,92)	24,64 (4,05)	ANOVA (n.s.)
Lignin	23,11 (1,59)	22,93 (2,23)	22,95 (1,92)	ANOVA (n.s.)
Extractives	1,71 (16,18)	1.90 (16,82)	1,75 (12,38)	ANOVA (n.s.)
Ash	0,77 (4,76)	0,8 (0,36)	0,76 (2,05)	Kruskal- Wallis (n.s.)
Silica	0,26 (17,39)	0,20 (3,66)	0,25 (20,75)	ANOVA (n.s.)
Note: Data are expressed in percentage, where (n.s.) denotes not significant. Coefficient of variation ().				

Although no significance was found among the obtained values, the high zone exhibited slightly higher values for cellulose and lignin content. The high zone of the trunk contains a higher proportion of juvenile wood, which is characterised by the presence of more cellulose and, also, a greater chemical accessibility to extract a larger amount of lignin. The opposite occurs in the lower zone of the trunk, where the wood has a higher degree of lignification and is more reticulated (Malpartida 2010). The growth site of the species should also be considered, as it will influence the lignin constituents through its structure and chemistry (César *et al.* 2019, Katahira *et al.* 2018).

The results show a low lignin concentration, which is related to the early age of the tree because, according to Zaki *et al.* (2012), this concentration increases as the tree ages owing to its need to harden and become more resistant.

A low level of extractives, < 2 %, is ideal for the pulping process. Honorato *et al*. (2015) mention that a high percentage of extractives in wood makes it an undesirable material for pulping because it negatively influences delignification during digestion and also forms coloured complexes that affect the whiteness of the pulp.

Obtaining and bleaching cellulosic pulp

The cellulosic pulp yields for the different shaft sections were in the 45 % – 47 % range, which correspond to the yield (40 % – 55 %) reported by Bajpai (2018) for soda digestion (Table 3).

Table 3: Results of the digestion and bleaching process of bolaina blanca cellulosic pulp.

Shaft section	Pulping yield (%)	Bleaching yield (%)
Basal section	45,54 (n.s.) (15,45)	83,79(n.s.) (10,33)
Middle section	47,01(n.s.) (6,61)	87,53(n.s.) (6,91)
High section	45,95 (n.s.) (11,35)	85,63 (n.s.) (8,29)

Note: n.s.: Not significant, Coefficient of variation (). No significant differences were observed between pulping and bleaching yield averages among shaft sections.

The yield of the digestion process indicates nearly complete solubilisation of the non-cellulosic elements. According to the results listed in Table 2, bolaina blanca wood at different sections contained approximately 52 % cellulose. The low yield obtained from the pulping process in general results from the partial degradation of amorphous/soluble cellulose (beta and gamma cellulose) due to the parameters used, yielding a pulp with a high percentage of alpha-type cellulose, which is characterised by its insolubility in sodium hydroxide, stability and high crystallinity (Manzano 2021, Singh *et al.* 2021).

Bleaching yields vary between 90 % and 97 % (Bajpai 2018). The yield obtained in this study was between 82,3 % and 87,9 %. This low yield was caused by the loss of white pulp due to the intensity of bleaching with consequent removal of pulp mass, mainly residual lignin and low molecular weight carbohydrates such as hemicelluloses.

The Kappa index test indicates the delignification caused by the bleaching process. The unbleached pulp had a residual lignin content of 4,28 %, which decreased to < 1 % after bleaching. The delignification of the white pulp reached a value of 98,22 %, demonstrating the efficiency of the stepwise process.

Measurement of anatomical elements of interest *Guazuma crinita* fibres

Fibre length showed significant differences in the basal section with a value of 1322 µm with respect to the middle and high sections (Table 4). The length reached an average value of 1156 µm with respect to the three sections, which can be catalogued as medium length fibres according to the International Association of Wood Anatomy (IAWA 1989). However, the fibre diameter exhibited significant differences in the upper section, with a value of 28,77 µm, compared with the middle and basal sections; classified in the category of medium diameter fibres according to IBAMA (1991). Similar values for the species studied were reported by Córdova *et al*. (2020). Cell wall thickness averaged 3,91 µm, showing no significant differences among the three sections. Beeckman (2016) mentions that the environment influences both the growth and quality of the anatomical elements of wood, whereas Rodríguez *et al*. (2015) point out that the treatment conducted to separate the anatomical elements will have an influence on fibre measurement results.

Table 4: Measurements of bleached chemical pulp fibres.

Measurement of the fibres anatomical elements					
	High S.	**Middle S.**	**Basal S.**	**Average**	**Test**
Length (µm)	1087(b) (12,56)	1059(b) (15,87)	1322(a) (13,99)	1156	Tukey
Overall diameter (µm)	30,10(a) (16,86)	29,77(a) (20,51)	26,44(b) (22,33)	28,77	Kruskal–Wallis
Wall thickness (µm)	3,61(n.s.) (25,62)	4,39(n.s.) (30,30)	3,72(n.s.) (36,25)	3,91	ANVA
Lumen diameter (µm)	17,22(b) (10,43)	16,59(c) (20,86)	18,17(a) (35,95)	17,33	Kruskal–Wallis
Note: Means that do not share a letter are significantly different. n.s.: Not significant. Coefficient of variation ().					

Obtaining and lyophilising CNF

CNF was obtained in a solution at a consistency of 1,5 % (w/w). The yield was calculated for freeze-drying the solution to obtain dry NCF. The yield was approximately 96 % from

the milling of the cellulosic pulp. These results are consistent with the proper proportion of cellulose in the pulp.

The high, middle and basal sections achieved average cumulative yields (of the entire transformation from log to CNF) of 32,1 %, 33,6 % and 31 %, respectively.

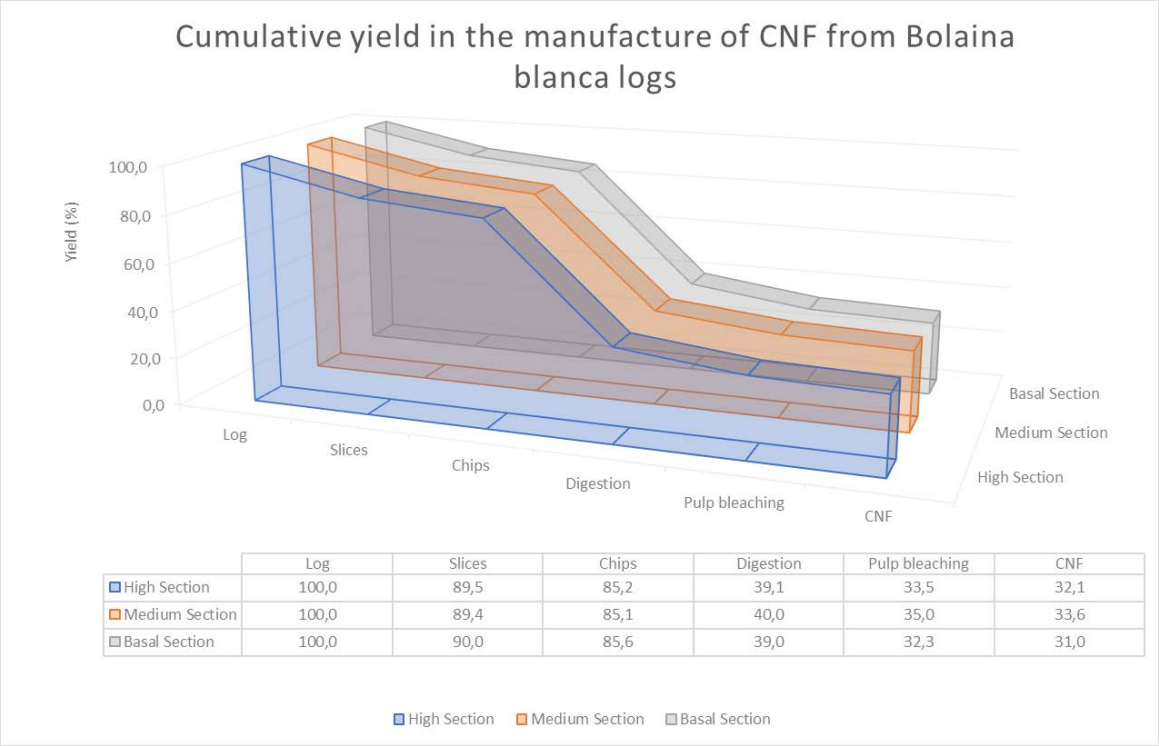

	Log	Slices	Chips	Digestion	Pulp bleaching	CNF
High Section	100,0	89,5	85,2	39,1	33,5	32,1
Medium Section	100,0	89,4	85,1	40,0	35,0	33,6
Basal Section	100,0	90,0	85,6	39,0	32,3	31,0

Figure 1: Cumulative performance in obtaining CNF from bolaina blanca logs.

CNF characterisation

Determination of polymerisation degree (DP) of CNF

The DP of CNF presented significant differences in all the sections of origin. The values were 300, 249 and 211 for the basal, middle and high sections, respectively. A decrease in the DP of CNF was evidenced as the height of the section of origin increased.

This coincides with the discussion by Carballo *et al*. (2004), which mentions that, at greater stem height, fibres are less cross-linked with each other owing to a lower lignin content and less fibre development, thereby suggesting a lower DP of their composing monomeric units.

Tárres (2017) obtained DP values in the range between 300 and 450 for CNF from Eucalyptus via enzymatic hydrolysation (Endo-β-1,4-glucanase); Megashah *et al*. (2020) obtained DP values of 500 for oil palm CNF obtained using mechanical treatments such as disc milling, and Hu *et al*. (2015) obtained a DP of 660 for CNF from *Eucalyptus*. These results show that DP varies according to the material from which CNF is obtained and the treatment used for CNF production. In this context, the large-scale decrease in the obtained DP (between 210 and 300) was mainly due to the treatments to which the wood was subjected until obtaining CNF, with large influence mainly of the digestion, bleaching and final mechanical milling processes.

Scanning electron microscopy

The Figure 2.A denotes the nanofibrils (indicated by red arrows) with a morphology very similar to the original fibres, but at a nanometer size in diameter, which may be due to the delignification level higher than 98 %, reason for which the nanofibrils had greater feasibility to be released by the shear forces produced by the impact of the moving balls on the paste.

Figure 2.B depicts the nanofibrils released from the original fibres, which formed a network-like structure. Moreover, Figure 2.C depicts rough surfaces (enclosed in red circles) that were present on the nanofibrils. Ramesh and Radhakrishnan (2019) have reported that surface roughness is due to the dissolution of lignin and hemicellulose compounds, removed during the alkaline hydrolysis and bleaching process. The appearance of roughness resulting from the loss of non-cellulosic components is due to sedimentation of the fibres in the plant cell wall by these components; consequently, when these components are removed, they leave the fibrils worn.

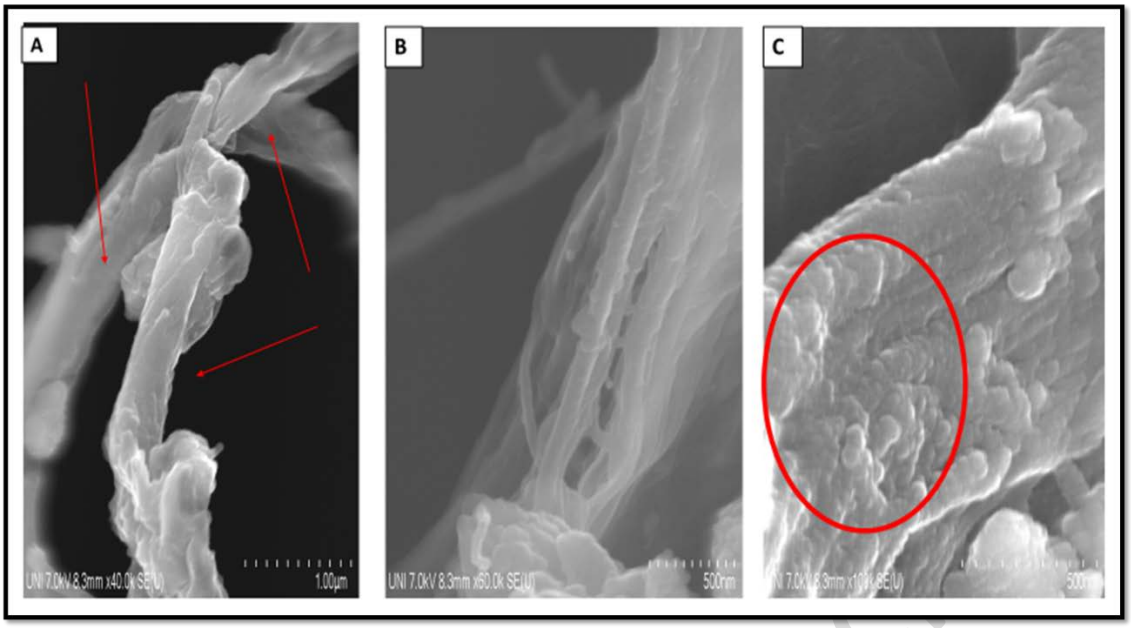

Figure 2: SEM micrographs of CNF of Bolaina blanca wood from different sections. A) Cellulosic microfibril, B) Macrofibril defibrillation and C) Microfibril roughness.

Table 5 lists the average diameter values of the nanofibrils that were measured with origin in the different sections of interest.

Table 5: CNF diameter.

Section	N	Average diameter Mann - Whitney(nm)
High section	62	84 (a) (64,99)
Medium section	44	75 (b) (54,92)
Basal section	48	69 (b) (51,5)

Note: N is the number of nanofibril bundles measured per section. Coefficient of variation (). Means that do not share a letter are significantly different.

Generally, nanofibrils with average diameters < 100 nm was obtained. Importantly, the diameter of the nanofibrils originating in the high section was larger than that of the nanofibrils originating in the middle and basal sections.

The results contrasted with those reported by Ponce *et al*. (2020), who obtained NCF from Tara with diameters of 300 nm using the same equipment for mechanical treatment, presenting higher values than those obtained in this study. This may be because they did not perform pulp bleaching; therefore, fibres were compacted even by the remaining

lignin during defibrillation. Conversely, Siró and Plackett (2010) obtained NC from bleached pine pulp with diameters between 10 nm and 100 nm using a high-pressure homogeniser.

The difference in results with respect to those obtained by other authors is due to the different conditions during the mechanical disintegration of the cellulosic pulp, validating the study conducted by Fukuzumi *et al*. (2013), who assessed the dimensional change of the nanofibrils before evaluating different milling parameters.

Fourier transform infrared (FTIR) spectroscopy

Infrared (IR) spectra corresponding to each section were analysed using the averages of the absorbance obtained in the spectral range of 400 cm^{-1} – 4000 cm^{-1}. Figure 3 depicts the FTIR spectra of the CNF obtained from the high, middle and basal sections.

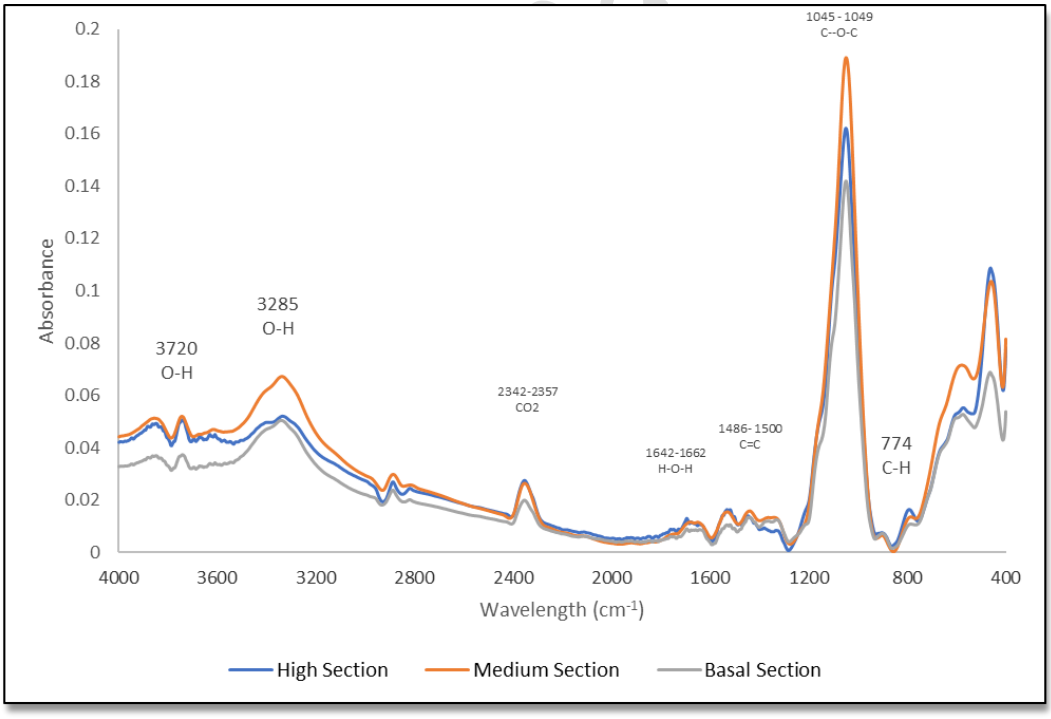

Figure 3: Infrared (IR) spectra of high, medium and basal section of CNF of bolaina blanca.

The C–H bonds (770 cm^{-1} to 880 cm^{-1}) directly related to the vibrations of glycosidic bonds of glucose monomers were evidenced, which were also possible indicators of the remaining amorphous zone of cellulose (Hospodarova *et al.* 2018).

In this study, we were able to verify the presence of C–O–C bonds (1045 cm^{-1} – 1049 cm^{-1}) corresponding to the pyranose rings constituting cellulose, C=C bonds (1475 cm^{-1} – 1600 cm^{-1}) originating from the aromatic rings of lignin and CO_2 (weak absorptions very close to 2346 cm^{-1}), as CO_2 can be easily added on the surface of the study material through the adsorption phenomenon.

Furthermore, O–H bonds peaks (3000 cm^{-1} to 4000 cm^{-1}) originated from the hydroxyls present in the cellulose molecules in addition to the O–H bonds (1631 cm^{-1} – 1665 cm^{-1} and 3311 cm^{-1} – 3329 cm^{-1}) typical of the hydrogen bridge characteristic of intermolecular bonds between cellulose chains. For these bonds, the absorptions were weak because the water in the CNF was removed via freeze-drying (Larkin 2018, Mandal and Chakrabarty 2011, Oancea *et al.* 2012, Rigg 2018). Additionally, the vibrational peak at 1049 cm^{-1} denotes a large stretch related to cellulose crystallinity (Elanthikkal *et al.* 2010, Hospodarova *et al.* 2018). Moreover, nearby peaks are present between 1630 cm^{-1} and 1730 cm^{-1}, which are representations of vibrations corresponding to acetyl and uronic ester bonds of hemicellulose and ester bonds present in carboxylic groups of lignin (Johar *et al.* 2012, Kumar *et al.* 2014).

As evidenced, the NaOH treatments during digestion and the NaClO and H_2O_2 used in bleaching had considerable effect on the oxidation and partial removal of non-cellulosic elements.

The IR spectra patterns showed no differences among the three zones, coinciding with the chemical characterisation (Table 1).

X-ray diffraction

From the obtained diffractograms (Figure 4), it was observed that the most distinct peaks were those present at 2θ = 15,7°; 22,5° and 34,7°, which correspond to (110), (200) and (004) crystalline planes respectively, typical of type Iβ cellulose. Moreover, this trend of peaks was much more evident for the basal and middle zones. For the high zone, no intensity peaks were found for 2θ = 15,7° but for 2θ = 12,7° and 14,4°, which were associated with the (110) plane of a crystalline region characteristic of type II cellulose [14]. Based on the aforementioned X-ray diffraction observations, we inferred that the chemical treatment performed for the release of cellulose from other compounds exerted a more substantial effect on the high zone by disordering and/or somehow affecting the crystallinity of its structure.

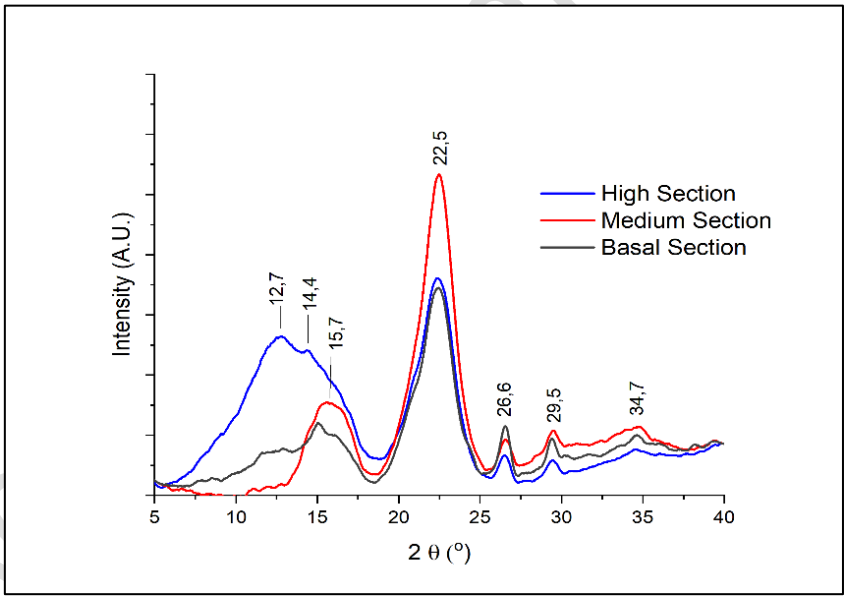

Figure 4: CNF diffractograms of bolaina blanca obtained from three different sections of the longitudinal axis of the shaft.

The highest degree of crystallinity (IC) was obtained from the basal section with a value of 96 % (crystal diameter = 3,4 nm), followed by the middle zone with a value of 93 % (crystal diameter = 3,6 nm) and the high zone with a value of 76 % (crystal diameter =

3,4 nm). No correlation was found between the IC and the average crystal size of each CNF sample from each longitudinal section of the tree. Crystallinity values were high owing to the successive chemical treatments conducted to obtain CNF, which caused a decrease in the amorphous zones.

Overall, the obtained crystallinity index was above the crystallinity index range reported by Campano *et al*. (2016), who mention that for a fibrillar nanocellulosic material to have good mechanical and physical properties, the crystallinity index must be between 84 % and 89 %. The decrease in CNF crystallinity with respect to the increase in shaft height exhibited the same trend with respect to DP. Hence, the number of monomers composing the cellulosic chain had a direct influence on the IC.

Thermogravimetric analysis

The decomposition of the NCF started from 250 °C and culminated at approximately 360 °C. In this range, the highest amount of mass (volatile material) was released with 82,1 %, 83,7 % and 82,3 % for the CNF from the high, middle and basal sections, respectively, for which these results did not show significant differences (Figure 5).

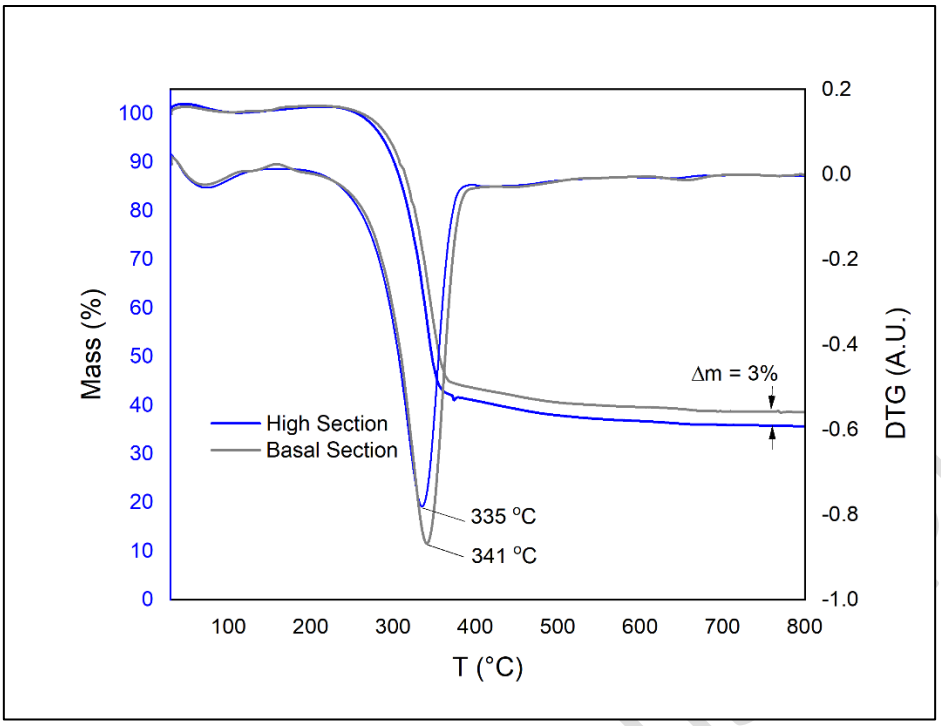

Figure 5: CNF thermograms obtained from the high and basal sections.

The temperature corresponding to the maximum decomposition rate for the CNF from the basal zone (341 °C) was higher with respect to that for the CNF from the high zone (335 °C), with a difference of 6 °C, where the sample from the apex lost a slightly higher mass percentage (approximately 3 %) than the sample from the base. This is due higher crystallinity values are related with lowest thermal degradation stability in CNF and CNC (Yildirim and Shaler 2017). This trend was related to the nanofibrils of the basal zone being more developed than those of the apex, which was corroborated by the polymerisation and crystallinity degree results because the sample of this zone was more rigid and therefore might have needed more energy for its decomposition compared with the high CNF.

Ultraviolet–visible spectroscopy

407 The results of methylene blue adsorption by CNF from different sections validate an
408 efficiency > 60 % for the removal of methylene blue at different concentrations (10 ppm
409 and 20 ppm) using CNF at two different weights of 50 mg and 100 mg (Table 6).

410 **Table 6.**: Methylene blue removal values at different concentrations using CNF.

Initial concentration of methylene blue	Adsorbent mass	Section	Ce (mg/L)	qe (mg/g)
20 mg/L	50 mg	High	9,51	10,34
		Medium	10,06	9,97
		Basal	9,89	9,98
	100 mg	High	6,74	6,51
		Medium	7,07	6,47
		Basal	7,56	6,17
10 mg/L	50 mg	High	3,84	6,83
		Medium	4,14	6,52
		Basal	4,34	6,21
	100 mg	High	2,96	3,85
		Medium	3,04	3,78
		Basal	3,55	3,51
Ce: Equilibrium concentration and qe: Specific adsorption.				

411

412 The adsorption capacity was considerably higher in the high zone with a value of 65 %,
413 followed by the middle and basal zones, with values of 62 % and 61 %, respectively. This
414 was due to the CNF from the high zone containing a higher proportion of amorphous zone
415 in its structure, indicated by its much lower crystallinity index than the middle and basal
416 zones; therefore, it has more availability to generate bonds with the molecules that
417 compose the methylene blue reagent. Moreover, Keplinger *et al*. (2019) have reported
418 that the adsorption capacity is influenced by the type of drying performed on NC,
419 according to which supercritical drying as the lyophilisation used in this study yields
420 better results by retaining the porous structure of NC without the use of any solvent.

421 By increasing the initial concentration of adsorbate (methylene blue) from 10 pm to 20
422 ppm, the removal percentage decreased from 61,6 % to 50,8 % and from 70,2 % to 64,3
423 % for the adsorbent masses of 50 mg and 100 mg CNF, respectively. Because at a higher

availability of available adsorption sites at low concentrations of the adsorbate, much of methylene blue molecules can be removed more effectively. However, when the initial concentration of the adsorbate is increased, the competition to attach to the available sites among the methylene blue molecules increases, and even after reaching equilibrium, these molecules remain in the solution, which reduces the removal percentage (Ahmad and Alrozi 2010, Rangabhashiyam *et al.* 2014).

CONCLUSIONS

CNF was obtained from bleached cellulosic pulp of Bolaina blanca wood (*Guazuma crinita*) from different shaft sections. The wood to CNF yields were higher than 32 % for the different sections of the longitudinal axis of the shaft from which it was obtained.

CNF obtained from the different sections generally had a diameter < 90 nm. CNF from the high section had a considerably larger diameter than CNF from the middle and basal sections.

CNF from the basal section exhibited a considerably higher degree of polymerisation, more crystallinity and better thermostability. Moreover, CNF from the high section exhibited considerably better methylene blue dye adsorption condition.

AUTHORSHIP CONTRIBUTIONS

S. A. A-P.: Data curation, formal analysis, investigation, methodology, software, validation, visualization, writing – original draft, writing – review & editing**. H. E. G-M:** Conceptualization**,** funding acquisition, supervision, project administration, resources, methodology, writing – original draft, writing – review & editing**. S. P. P-A.:** Writing – review & editing. **A. A. G-E.:** Writing – review & editing. **A. J. C-O.:** Conceptualization, funding acquisition, supervision, methodology, project administration, resources, writing – original draft, Writing – review & editing**.**

ACKNOWLEDGEMENTS

This work was elaborated thanks to the support of 009-2020-FONDECYT- BM project - Development of biodegradable and antibacterial packaging paper using a bilayer film based on nanocellulose from forest residues of Bolaina (*Guazuma crinita*) with the incorporation of copper nanoparticles for the food industry.

REFERENCES

Ahmad, A.; Alrozi, R. 2010. Optimization of preparation conditions for Mangosteen peel-based activated carbons for the removal of Remazol brilliant blue R using response surface methodology. *Chem Eng J* 165(3): 883-890. https://doi.org/10.1016/j.cej.2010.10.049

American Society for Testing and Materials. 2015. ASTM D7582-15. Standard test methods for proximate analysis of coal and coke by macro thermogravimetric analysis. ASTM International, West Conshohocken, Pensilvania, United States. https://www.astm.org/d7582-12.html

Bajpai, P. 2018. Chapter 12. Pulping Fundamentals. In: *Handbook of pulp and paper* (Third Ed.). Elsevier. https://doi.org/10.1016/B978-0-12-814240-0.00012-4

Beeckman, H. 2016. Wood anatomy and trait-based ecology. *IAWA J* 37(2): 127-151. https://doi.org/10.1163/22941932-20160127

Borjesson, M.; Westman, G. 2015. Chapter 7. Crystalline nanocellulose—preparation, modification and properties. In: *Cellulose - Fundamental Aspects and Current Trends*. IntechOpen. http://dx.doi.org/10.5772/61899

Campano, C.; Balea, A.; Blanco, A.; Negro, C. 2016. Enhancement of the fermentation process and properties of bacterial cellulose: a review. *Cellulose* 23(1): 57-91. https://doi.org/10.1007/s10570-015-0802-0

Carballo, L.; Orea, U.; Cordero, E. 2004. Composición química de tres maderas en la provincia de Pinar Del Río, CUBA a tres alturas del fuste comercial, Parte 4: Estudio comparativo de la composición química. *Chapingo* 10(2): 77-81. https://revistas.chapingo.mx/forestales/?section=articles&subsec=issues&numero=30&articulo=414 (In Spanish)

Césare, M.; Hilario, F.; Callupe, N.; Cruz, L.; Caller, J., Gonzales, H. 2019. Caracterización química Y física del bambú. *Av Cien Ing* 10(4): 1-13. https://www.executivebs.org/publishing.cl/aci/2019/Vol10/Nro4/1-ACI1336-19-full.pdf (In Spanish)

Cipra Rodriguez, J.A.; Gonzales Mora, H.E.; Cárdenas Oscanoa, A.J. 2022. Characterization of MDF produced with bolaina (*Guazuma crinita* Mart.) wood residues from plantation. *Madera Bosques* 28(3): e2832433. https://doi.org/10.21829/myb.2022.2832433

Córdova, A.; Cárdenas, A.; Gonzáles, H. 2020. Caracterización física y mecánica de compuestos de *Guazuma crinita Mart*. a base de polipropileno virgen. *Rev Mex Cienc For* 11(57): 1-28. https://doi.org/10.29298/rmcf.v11i57.621 (In Spanish)

Elanthikkal, S.; Gopalakrishnapanicker, U.; Varghese, S.; Guthrie, J.T. 2010. Cellulose microfibres produced from banana plant wastes: Isolation and characterization. *Carbohyd Polym* 80(3): 852-859. https://doi.org/10.1016/j.carbpol.2009.12.043

Fukuzumi, H.; Saito, T.; Isogai, A. 2013. Influence of TEMPO- oxidized cellulose nanofibril length on film properties. *Carbohyd Polym* 93: 172-177. https://doi.org/10.1016/j.carbpol.2012.04.069

Habibi, Y. 2014. Key advances in the chemical modification of nanocelluloses. *Chem Soc Rev* 43(5): 1519-1542. https://doi.org/10.1039/C3CS60204D

Herrera, M. 2018. Obtención de nanocelulosa a partir de celulosa de puntas de abacá. Engineering thesis. Escuela Politécnica Nacional. Quito, Ecuador. https://bibdigital.epn.edu.ec/handle/15000/19544 (In Spanish)

Honorato, A.; Colotl, G.; Apolinar, F.; Aburto, J. 2015. Principales componentes químicos de la madera de Ceiba pentandra, *Hevea brasiliensis* y *Ochroma pyramidale*. *Maderas Bosques* 21(2): 131-146. https://doi.org/10.21829/myb.2015.212450 (In spanish)

Hospodarova, V.; Singovszka, E.; Stevulova, N. 2018. Characterization of Cellulosic Fibers by FTIR Spectroscopy for Their Further Implementation to Building Materials. *Am J Anal Chem* 9(6): 303-310. https://doi.org/10.4236/ajac.2018.96023

Hu, C.; Zhao, Y.; Li, K.; Zhu, J.Y.; Gleisner, R. 2015. Optimizing cellulose fibrillation for the production of cellulose nanofibrils by a disk grinder. *Holzforschung* 69(8): 993-1000. https://doi.org/10.1515/hf-2014-0219

International Association of Wood Anatomists. IAWA. 1989. *IAWA list of microscopic features for hardwood identification with an appendix on non-anatomical information.* Wheeler, E.A.; Baas, P.; Gasson, P.E. (Eds.). Published for the International Association of Wood Anatomists at the National Herbarium of the Netherlands, Leiden. *IAWA J* 10(3): 219-332. https://www.iawa-website.org/uploads/soft/Abstracts/IAWA%20list%20of%20microscopic%20features%20for%20hardwood%20identification.pdf

Instituto Brasileiro do Meio Ambiente e Dos Recursos Naturais Renovaveis. IBAMA. 1991. Normas de procedimentos em estudos do anatomía do madeira: I. Angiospermae. 19 p. https://lpf.florestal.gov.br/pt-br/publicacoes-tecnicas-do-lpf/72-

519 normas-de-procedimentos-em-estudos-de-anatomia-de-madeira-i-angiospermae-ii-
520 gimnospermae (In Portuguese)

521 **Johar, N.; Ahmad, I.; Dufresne, A. 2012**. Extraction, preparation and characterization
522 of cellulose fibres and nanocrystals from rice husk. *Ind Crop Prod* 37(1): 93-99.
523 https://doi.org/10.1016/j.indcrop.2011.12.016

524 **Kargarzadeh, H.; Ioelovich, M.; Ahmad, I.; Thomas, S.; Dufresne, A. 2017.** Methods
525 for extraction of nanocellulose from Various Sources. Chapter 1. In: *Handbook of*
526 *nanocellulose and cellulose Nanocomposites.* Wiley-VCH.
527 https://doi.org/10.1002/9783527689972.ch1

528 **Katahira, R.; Elder, T.J.; Beckham, G.T. 2018.** Brief introduction to lignin structure.
529 Chapter 1. In: *Lignin Valorization: Emerging Approaches*. Beckham, G.T. (Ed.). Energy
530 and Environment Series No. 19. 1-20. The Royal Society of Chemistry.
531 https://doi.org/10.1039/9781788010351-00001

532 **Keplinger, T.; Wang, X.; Burgert, I. 2019.** Nanofibrillated cellulose composites and
533 wood derived scaffolds for functional materials. *J Mater Chem A* 7: 2981-2992.
534 https://doi.org/10.1039/c8ta10711d

535 **Kumar, A.; Negi, Y.S.; Choudhary, V.; Bhardwaj, N.K. 2014**. Characterization of
536 cellulose nanocrystals produced by acid-hydrolysis from sugarcane bagasse as agro-
537 waste. *J Mater Phys Chem* 2(1): 1-8. https://doi.org/10.12691/jmpc-2-1-1

538 **Larkin, P.J. 2018**. IR and Raman Spectra–Structure Correlations: Characteristic Group
539 Frequencies. Chapter 6. In: *Infrared and Raman spectroscopy: principles and spectral*
540 *interpretation.* Second Ed. 85-134p. Elsevier International Publishing.
541 https://doi.org/10.1016/B978-0-12-804162-8.00006-9

Lee, K.Y.; Tang, M.; Williams, C.K.; Bismarck, A. 2012. Carbohydrate derived copoly(lactide) as the compatibilizer for bacterial cellulose reinforced polylactide nanocomposites. *Compos Sci Tecnol* 72(14): 1646–1650. https://doi.org/10.1016/j.compscitech.2012.07.003

Lermen, A.M.; Fronza, C.S.; Diel, J.C.; Schein, D.; Clerici, N.J.; Guimarães, R.E.; Boligon, S.D.; Scher, A.C. 2021. A utilização de resíduos agroindustriais para adsorção do corante azul de metileno: uma breve revisão. *BASR* 5(1): 273-288. https://doi.org/10.34115/basrv5n1-017 (In Portuguese)

Malpartida, I. 2010. Determinación de la composición química de la especie bolaina blanca (*Guazuma crinita* Mart.) procedente del sector cadena- Tingo María. Engineering thesis, Universidad Nacional Agraria de la Selva. Tingo María, Perú. http://repositorio.unas.edu.pe/bitstream/handle/UNAS/556/T.FRS-159.pdf?sequence=1&isAllowed=y (In Spanish)

Mandal, A.; Chakrabarty, D. 2011. Isolation of nanocellulose from waste sugarcane bagasse (SCB) and its characterization. *Carbohyd Polym* 86(3): 1291-1299. https://doi.org/10.1016/j.carbpol.2011.06.030

Manzano, D. 2021. Extracción de celulosa a partir de la especie *Calamagrostis intermedia* para la preparación de compuestos semisintéticos, Master Thesis, Universidad Técnica de Ambato. Ambato, Ecuador. https://repositorio.uta.edu.ec/jspui/handle/123456789/32958 (In Spanish)

Megashah, L.; Ariffin, H.; Zakaria, M.; Hassan, M.; Andou, A.; Padzil, F. 2020. Modification of cellulose degree of polymerization by superheated steam treatment for

564 versatile properties of cellulose nanofibril film. *Cellulose* 27(13): 7417-7429.
565 https://doi.org/10.1007/s10570-020-03296-2

566 **Miguel, M.; Iwakiri, S.; Trianoski, R.; Gonzales, H.; Miguel, C. 2019**. Producción de
567 tableros de partículas con bolaina (*Guazuma crinita Mart*.) procedente de una plantación
568 de cuatro años. *Braz Wood Sci* 10(2): 197-204. https://doi.org/10.12953/2177-
569 6830/rcm.v10n3p197-204 (In Spanish)

570 **Siddiqui, N.; Mills, R.; Gardner, D.; Bousfield, D. 2011**. Production and
571 Characterization of Cellulose Nanofibers from Wood Pulp. *J Adhes Sci Technol* 25(6-
572 7): 709-721. https://doi.org/10.1163/016942410X525975

573 **Oancea, A.; Grasset, O.; Le Menn, E.; Bollengier, O.; Bezacier, L.; Le Mouelic, S.;**
574 **Tobie, G. 2012**. Laboratory infrared reflection spectrum of carbon dioxide clathrate
575 hydrates for astrophysical remote sensing applications. *Icarus* 221(2): 900-910.
576 https://doi.org/10.1016/j.icarus.2012.09.020

577 **Ozen, E.; Yildirim, N.; Dalkilic, B.; Ergun, M. 2021**. Effects of microcrystalline
578 cellulose on some performance properties of chitosan aerogels. *Maderas-Cienc Tecnol*
579 (23): 26, 1-10. https://dx.doi.org/10.4067/s0718-221x2021000100426

580 **Rangabhashiyam, S.; Anu, N.; Giri, M.; Selvaraju, N. 2014.** Relevance of isotherm
581 models in biosorption of pollutants by agricultural byproducts. *J Environ Chem Eng* 2(1):
582 398-414. https://doi.org/10.1016/j.jece.2014.01.014

583 **Rodríguez, R.; Ramírez, A.; Palacios, H.; Fuentes, F.; Silva, J., Saucedo, A. 2015.**
584 Características anatómicas, físico-mecánicas y de maquinado de la madera de mezquite
585 (*Prosopis velutina* Wooton). *Rev Mex Cienc For* 6(28): 156-173.
586 https://www.scielo.org.mx/scielo.php?script=sci_arttext&pid=S2007-
587 11322015000200011 (In Spanish).

588 **Ponce, S.; Chavarria, M.; Norabuena, F.; Chumpitaz, D.; Gutarra, A. 2020**.
589 Cellulose microfibres obtained from agro-industrial Tara waste for dye adsorption in
590 water. *Water Air Soil Pollut* 231: 518. https://doi.org/10.1007/s11270-020-04889-0

591 **Ramesh, S.; Radhakrishnan, P. 2019**. Cellulose nanoparticles from agro-industrial
592 waste for the development of active packaging. *Appl Surf Sci* 484: 1274-1281.
593 https://doi.org/10.1016/j.apsusc.2019.04.003

594 **Revilla, J. 2015**. Viabilidad económica de plantaciones demostrativas de Bolaina blanca
595 (*Guazuma crinita* C. Mart.) en la cuenca del rio Aguaytía, Ucayali -Perú. Master Thesis,
596 Escuela de Posgrado, Universidad Nacional Agraria la Molina. Lima, Perú
597 http://repositorio.lamolina.edu.pe/handle/20.500.12996/2119 (In Spanish)

598 **Rigg, P. 2018**. Efecto de la adición de micro-nanocelulosa cristalina en adhesivos y su
599 aplicación en aglomerados de madera de especies forestales tropicales. Master Thesis,
600 Escuela de Ingeniería Forestal, Instituto Tecnológico de Costa Rica. Cartago, Costa Rica.
601 https://repositoriotec.tec.ac.cr/bitstream/handle/2238/9783/efecto_adición_micronanoce
602 lulosa_cristalina_adhesivos.pdf?sequence=1&isAllowed=y (In Spanish)

603 **Segal, L.; Creely, J.; Martin, A.; Conrad, C. 1959**. An empirical method for estimating
604 the degree of crystallinity of native cellulose using the X-ray diffractometer. *Text Res J*
605 29(10): 786-764. https://doi.org/10.1177/004051755902901003

606 **Singh, K.; Matsagar, B.; Dhepe, P. 2021.** Determination of alpha-, beta-and gamma-
607 cellulose in bagasse and wheat Straw: lignin recovery, characterization and
608 depolymerization. *Clean Technol Environ Policy* 19: 23-29.
609 https://doi.org/10.21203/rs.3.rs-193157/v1

610 **Siró, I.; Plackett, D. 2010**. Microfibrillated cellulose and new nanocomposite materials:
611 a review. *Cellulose* 17(3): 459–494. https://doi.org/10.1007/s10570-010-9405-y

612 **Technical Association of the Pulp and Paper Industries. 2008.** Viscosity of pulp
613 (capillary viscometer method). TAPPI T230 om-08. The Technological Association of
614 the pulp and paper Industry. Atlanta, GA, USA.
615 https://webstore.ansi.org/Standards/TAPPI/230om08

616 **Technical Association of the Pulp and Paper Industries. 2007.** Solvent extractives of
617 wood and Pulp. TAPPI T 204 om**.** The Technological Association of the pulp and paper
618 Industry. Atlanta, GA. USA. https://www.tappi.org/content/sarg/t204.pdf

619 **Technical Association of the Pulp and Paper Industries. 1998.** Acid-insoluble lignin
620 in wood and Pulp. TAPPI T 222 om. The Technological Association of the pulp and paper
621 Industry. Atlanta, GA. USA. https://www.tappi.org/content/SARG/T222.pdf

622 **Technical Association of the Pulp and Paper Industries. 1993a.** Ash in wood, pulp,
623 paper and paperboard: combustion at 525°C. TAPPI T 211 om. The Technological
624 Association of the pulp and paper Industry. Atlanta, GA. USA.
625 https://www.tappi.org/content/sarg/t211.pdf

626 **Technical Association of the Pulp and Paper Industries. 1993b.** Kappa number of
627 pulp. TAPPI T 236 om. The Technological Association of the pulp and paper Industry.
628 Atlanta, GA, USA. https://tappi.micronexx.com/CD/TESTMETHODS/T236.pdf

629 **Tárres, J.A. 2017**. Endo-β-1,4-glucanasa para la fabricación de micro/nanocelulosa:
630 propiedades y aplicaciones. Doctoral thesis, Universitat de Girona. Girona, España.
631 http://www.tdx.cat/handle/10803/456211 (In Spanish)

632 **Trache, D.; Tarchoun, A.; Derradji, M.; Hamidon, T.; Masruchin, N.; Brosse, N.;**
633 **Hussin, M. 2020**. Nanocellulose: from fundamentals to advanced applications. *Front*
634 *Chem* 8: 392. https://doi.org/10.3389/fchem.2020.00392

635 **Yildirim, N.; Shaler, S. 2017.** A Study on Thermal and Nanomechanical Performance
636 of Cellulose Nanomaterials (CNs). *Materials* 10*:* 718.
637 https://doi.org/10.3390/ma10070718
638 **Zaki, J.; Muhammed, S.; Shafie, A.; Wan, W. 2012**. Chemical properties of juvenile
639 latex timber clone rubberwood trees. *MJAS* 16(3): 228-234.
640 http://mjas.analis.com.my/wp-content/uploads/2018/11/Junaiza.pdf